IEEE Access
Multidisciplinary ⋮ Rapid Review ⋮ Open Access Journal

Received February 4, 2022, accepted February 17, 2022, date of publication February 24, 2022, date of current version March 7, 2022.

Digital Object Identifier 10.1109/ACCESS.2022.3154411

Separated Flow Through a Gap Between Two Coaxial Peristaltic Tubes

ABD EL HAKEEM ABD EL NABY[1] AND A. H. EL-BAZ[2]
[1]Department of Mathematics, Faculty of Science, Damietta University, New Damietta 34517, Egypt
[2]Department of Computer Science, Faculty of Computers and Artificial Intelligence, Damietta University, New Damietta 34517, Egypt

Corresponding author: A. H. El-Baz (elbaz@du.edu.eg)

This work was supported by the Academy of Scientific Research and Technology (ASRT), Egypt, under Grant 6501.

ABSTRACT A peristaltic endoscope is a device that could locomote through curving and tortuous spaces where it has many real-life applications in different disciplines e.g., in the field of medicine, it helps in the process of catheterization in curved tubes which in turn relieve patient's pain. The aim of this paper is to study a trapping phenomenon at the centerline of a gap between inner peristaltic endoscope and outer peristaltic tube of a fluid with viscosity variation and a novel phenomenon of separated flow at the boundary of these tubes. For understanding these phenomena, we formulate the flow of a fluid with viscosity variation through the gap between two coaxial peristaltic tubes in cylindrical coordinates with neglecting Reynolds number and wave number. Explicit forms for the velocity field, pressure rise and friction forces on inner and outer peristaltic tubes in terms of radius ratio, flow rate, parameter of viscosity and occlusion have been obtained. A new comparison between a rigid endoscope and a peristaltic endoscope through the gastrointestinal tract has been made for the pressure rising and drag (friction) forces results. Also, we identify type of pumping for various physical parameters of interest. In addition, separated flow points are determined numerically by using computer algebra system.

INDEX TERMS Fluid with variable viscosity, Newtonian fluid, peristalsis, peristaltic endoscope, separated flow, trapping.

NOMENCLATURE

$\overline{r}_1,\ \overline{r}_2$	Dimensional wall surfaces of peristaltic endoscope and small intestine at any time respectively.
n	Radius ratio.
a	Radius of the small intestine at inlet.
b	Wave amplitude.
c	Wave speed.
λ	Wavelength.
$\overline{t}$	Dimensional time.
$(\overline{R},\ \overline{Z})$	Dimensional cylindrical fixed coordinates system.
$(R,\ Z)$	Non-dimensional cylindrical fixed coordinates system.
$(\overline{r},\ \overline{z})$	Dimensional cylindrical moving coordinates system.
$(r,\ z)$	Non-dimensional cylindrical moving coordinates system.
$r_1,\ r_2$	Non-dimensional wall surfaces of peristaltic endoscope and small intestine in the moving coordinates respectively.
$\delta = \frac{a}{\lambda}$	Wave number.
$\varphi = \frac{b}{a}$	Amplitude ratio.
$(\overline{U},\ \overline{W})$	Dimensional velocity components in the radial and axial directions respectively in fixed coordinates.
$(U,\ W)$	Non-dimensional velocity components in the radial and axial directions respectively in fixed coordinates.
$(\overline{u},\ \overline{w})$	Dimensional velocity components in the radial and axial directions respectively in moving coordinates.
$(u,\ w)$	Non-dimensional velocity components in the radial and axial directions respectively in moving coordinates.
F	Non-dimensional volume flow rate in the moving coordinates system.

The associate editor coordinating the review of this manuscript and approving it for publication was Yeliz Karaca.

This work is licensed under a Creative Commons Attribution 4.0 License. For more information, see https://creativecommons.org/licenses/by/4.0/

P	Pressure.
$\overline{Q}$	Dimensional instantaneous volume flow rate in the fixed coordinates system.
$\overline{q}$	Dimensional volume flow rate in the moving coordinates system.
$\hat{Q}$	Dimensional time mean flow in the fixed coordinates system.
Θ	Non- dimensional time mean flow in the fixed coordinates system.
μ_0	Constant viscosity coefficient on peristaltic endoscope.
α	Viscosity parameter.
ΔP_λ	Non- dimensional pressure rise.
$F_\lambda^{(i)}$	Non- dimensional friction force on the peristaltic endoscope.
$F_\lambda^{(o)}$	Non- dimensional friction force on the small intestine.
$k_i,\ c_i$	Constants.
z_s	Longitudinal component of separation points.

I. INTRODUCTION

Nowadays, there have been several attempts to use biological revelation as the basis for renovation of endoscopes. Several investigators, inspired by the flexible locomotion of snakes, have created new endoscopes that can bend in response to the activation of shape memory alloy wires [1], [2]. A peristaltic endoscope is a device that could locomote through curving and tortuous spaces. It has several applications in different disciplines e.g., in industry and medicine. It could be used to maintain and repair machines with complex internal plumbing. Medically, endoscopy and catheterization within the human body may be done using a peristaltic endoscope, see for example, Mangan *et al.* [1]. Studies on effects of a concentric and an eccentric catheter on peristaltic motion for Newtonian fluids have shown in literature [3], [4]. Shukla *et al.* [5] discussed the influence of peripheral-layer viscosity on peristaltic movement of a bio-fluid in uniform tube and channel using the long wavelength approximation as in Shapiro *et al.* [6]. Shapiro *et al.* [6] investigated the fluid mechanics of peristaltic pumping in connection with the function of systems such as ureter, gastro-intestinal tract, the small blood vessels, and other glandular ducts. They found that there were two physiologically significant phenomena called ''reflux'' and ''trapping'' in peristaltic flow.

From physiological point of view, it is known that the small intestine receives secretions from other organs such as stomach, pancreas, liver and the small intestine itself. This shows that the fluid viscosity on the wall of small intestine is less than that away from the wall. Hence, the viscosity is dependent on the radial distance. Thus, Srivastava *et al.* [7] studied the influence of viscosity variation and peristaltic transport of physiological fluid flow in non-uniform geometry. They found that the effect of increasing viscosity decreases flow rate. Abd El Naby *et al.* [8] discussed the hydro-magnetics flow of a fluid with viscosity variation in a uniform tube with peristalsis. Some other studies discussed both the influence of Newtonian and non-Newtonian fluids of varied viscosity and that of a rigid endoscope on peristaltic movement in absence and presence of a magnetic field as given in literature [9]–[16]. Rachid and Ouazzani [17] studied effects of the electro-magneto-hydrodynamics (EMHD) flow of a bi-viscosity fluid through a permeable medium between two deformable coaxial tubes with different phases and amplitudes. McCash *et al.* [18] studied effects of a Newtonian fluid with constant viscosity and a peristaltic endoscope on trapping by using a curvilinear coordinate system.

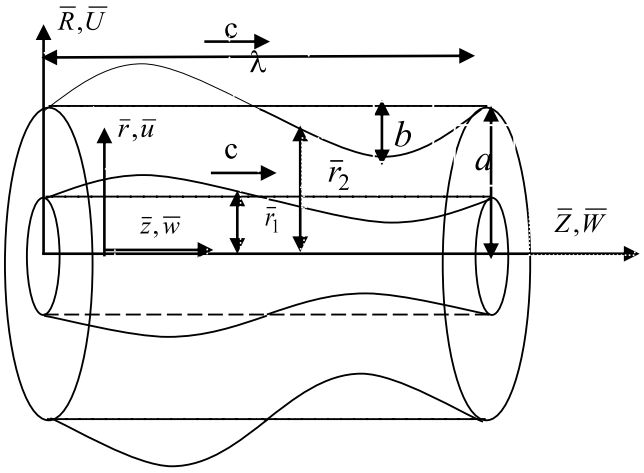

FIGURE 1. Peristaltic endoscope.

To the best of our knowledge, it is clear from previous studies that there is no attempt to study trapping and separated flow phenomena of a fluid with viscosity variation through the gap between two coaxial peristaltic tubes. So, this is the first study to explain these phenomena.

The paper is structured as follows. Section II gives the formulation of the problem in cylindrical coordinates in the non-dimensional form with canceling wave number and Reynolds number. In section III, trapping at the centerline of the gap has been studied. Separated flow (trapping at the boundary of the gap) has been studied in section IV. The peristaltic pumping, augmented pumping, trapping and separated flow have been discussed for various physical parameters of interest in section V. In section VI, concluding remarks are summarized.

II. FORMULATION OF THE PROBLEM

We investigate separation of creeping flow of a fluid with constant density and viscosity variation in a gap between two coaxial peristaltic tubes. The geometry of the walls surfaces is described in Fig. 1.

$$\overline{r}_1 = n\left(a + b\sin\frac{2\pi}{\lambda}\left(\overline{Z} - c\overline{t}\right)\right), \quad 0 < n < 1 \tag{1}$$

$$\overline{r}_2 = a + b\sin\frac{2\pi}{\lambda}\left(\overline{Z} - c\overline{t}\right), \tag{2}$$

where a is the radius of the outer peristaltic tube at entrance, b is the amplitude of the wave, λ is the wavelength, c is the wave speed, $\bar{t}$ is the time and n is radius ratio. If we select moving coordinates $(\bar{r}, \bar{z})$ which move in the $\overline{Z}$ direction with the same speed as the wave (wave frame), the tubes lengths are integral multiplied by wavelength, and the pressure difference through the gap between the two tubes is a constant so the flowing must be considered as steady flowing. The stationary and moving frames have been connected as follows:

$$\overline{Z} = \bar{z} + c\bar{t}, \quad \overline{R} = \bar{r}, \tag{3}$$

$$\overline{W} = \overline{w} + c, \quad \overline{U} = \overline{u}, \tag{4}$$

where $(\overline{u}, \overline{w})$ and $\left(\overline{U}, \overline{W}\right)$ are the velocity components in the radial and axial directions in the wave and laboratory frames, respectively.

Since the continuity equation in vector form is $\frac{\partial \rho}{\partial \bar{t}} + \vec{\nabla} \cdot \left(\rho \vec{V}\right) = 0$, momentum equation in vector form is

$$\rho \frac{D\vec{V}}{D\bar{t}} = -\vec{\nabla}\overline{P} + \vec{\nabla} \cdot \overline{\overline{\tau}} + \rho\vec{F}, \quad \overline{\overline{\tau}} = \mu\left(\vec{\nabla}\vec{V} + \left(\vec{\nabla}\vec{V}\right)^T\right),$$

where ρ is the density, $\vec{V}$ is the flow velocity in the stationary frame, $\overline{P}$ is the pressure, $\overline{\overline{\tau}}$ is Stokes' stress, μ is the dynamic viscosity, $\vec{F}$ is the body force per unit mass and $\bar{t}$ is time and boundary conditions in vector form are the tangential component of the fluid velocity on the wall is determined from no-slip boundary condition $\vec{V} \cdot \hat{e}_{\overline{Z}} = V_{wall}$ in the stationary frame, where $\hat{e}_{\overline{Z}}$ is the unit vector in the axial direction. Also, the normal component of the fluid velocity on the wall is determined from the boundary surface condition of a fluid $\frac{DF_i}{D\bar{t}} = 0$ at $\overline{R} = \overline{r}_i\left(\overline{Z}, \bar{t}\right), i = 1, 2$ with using the previous condition, where $F_i\left(\overline{R}, \overline{Z}, \bar{t}\right) = \overline{R} - \overline{r}_i\left(\overline{Z}, \bar{t}\right) = 0$. Then following [10], [14], [16] the governing equations of the flow with boundary conditions, under creeping flow ($\mathrm{Re} \ll 1$), long wavelength approximation ($\delta \ll 1$), the density is constant, the viscosity is variable, the flow is steady, the diameter Reynolds number is small $\left(\frac{\rho \overline{w} a}{\mu} \ll 1\right)$ and with negligence of gravitational force, in the wave frame in the non-dimensional form are continuity equation:

$$\frac{1}{r}\frac{\partial\left(ru\right)}{\partial r} + \frac{\partial w}{\partial z} = 0, \tag{5}$$

Navier-Stokes equations:

$$\frac{\partial P}{\partial r} = 0, \tag{6}$$

$$\frac{\partial P}{\partial z} = \frac{1}{r}\frac{\partial}{\partial r}\left(\mu\left(r\right) r \frac{\partial w}{\partial r}\right). \tag{7}$$

We neglect wave number by assuming that the wavelength is long compared to radius of the tube ($a \ll \lambda$), then ($\delta \ll 1$). Also, since the inertial force components in the dimensionless form for steady flow take the following form $\left(\mathrm{Re}\delta^3\left(u\frac{\partial u}{\partial r} + w\frac{\partial u}{\partial z}\right), \mathrm{Re}\delta\left(u\frac{\partial w}{\partial r} + w\frac{\partial w}{\partial z}\right)\right)$. Then ($\mathrm{Re}\delta \ll 1$), hence we may neglect the inertial terms. From the condition of boundary surfaces of a fluid, where the fluid particles originally on the walls must remain on the walls, and mechanical property of the walls in the stationary coordinates $\overline{W} = 0$ at $\overline{R} = \overline{r}_1, \overline{r}_2$. By using the transformations (3) and (4), we obtain the boundary conditions in the moving coordinates in the dimensionless form as follows:

$$w = -1 \quad at\ r = r_1, \tag{8a}$$

$$w = -1, \quad u = -\frac{dr_2}{dz}\ at\ r = r_2. \tag{8b}$$

Hence, the no-slip condition for a viscous flow is satisfied. The viscosity causes the fluid to stick to the walls and thus the velocity of the fluid at the walls assumes the velocity of the walls.

Where the dimensionless variables are given by

$$\begin{aligned}
&r = \frac{\overline{r}}{a}, \quad R = \frac{\overline{R}}{a}, \ r_1 = \frac{\overline{r}_1}{a} = n\left(1 + \varphi\sin\left(2\pi z\right)\right), \\
&z = \frac{\overline{z}}{\lambda}, \quad Z = \frac{\overline{Z}}{\lambda}, \ \mu\left(r\right) = \frac{\overline{\mu}\left(\overline{r}\right)}{\mu_0}, \ u = \frac{\lambda\overline{u}}{ac}, \\
&U = \frac{\lambda\overline{U}}{ac}, \quad w = \frac{\overline{w}}{c}, \ W = \frac{\overline{W}}{c}, \ \delta = \frac{a}{\lambda} \ll 1, \\
&P = \frac{a^2\overline{P}}{c\lambda\mu_0}, \quad t = \frac{c\bar{t}}{\lambda}, \ \varphi = \frac{b}{a} < 1 \text{ and} \\
&r_2 = \frac{\overline{r}_2}{a} = 1 + \varphi\sin\left(2\pi z\right),
\end{aligned} \tag{9}$$

where φ is the occlusion and μ_0 is the coefficient of viscosity on the surface of inner peristaltic tube. By integrating Eq. (7) and using the dimensionless boundary conditions (8), by using separation of variables method we can get the velocity profile as (10), shown at the bottom of the next page, where

$$I_1\left(r\right) = \int \frac{r}{\mu\left(r\right)} dr, \tag{11}$$

$$I_2\left(r\right) = \int \frac{dr}{r\mu\left(r\right)}. \tag{12}$$

The volume flow rate in the stationary and moving coordinates are given by

$$\overline{Q}\left(\overline{Z}, \bar{t}\right) = \int_{\overline{r}_1}^{\overline{r}_2} 2\pi\overline{R}\overline{W} d\overline{R}, \tag{13}$$

$$\overline{q} = \int_{\overline{r}_1}^{\overline{r}_2} 2\pi\overline{r}\overline{w} d\overline{r}. \tag{14}$$

By substitution from Eqs. (3) and (4) in Eq. (13) and making use of Eq. (14) gives

$$\overline{Q} = \overline{q} + \pi c\left(1 - n^2\right)\overline{r}_2^2. \tag{15}$$

The time-mean flowing through a period $T = \frac{\lambda}{c}$ at a stationary position $\overline{Z}$ is defined as:

$$\hat{Q} = \frac{1}{T}\int_0^T \overline{Q}\left(\overline{Z}, \bar{t}\right) d\bar{t}. \tag{16}$$

By substitution from Eq. (15) in Eq. (16) and integrating yields:

$$\hat{Q} = \overline{q} + \pi c \left(1 - n^2\right) \left(a^2 + \frac{b^2}{2}\right). \tag{17}$$

On defining the dimensionless time-mean flow Θ and the volume flow rate F in the wave frame as follows:

$$\Theta = \frac{\hat{Q}}{2\pi\, ca^2} \quad \text{and } F = \frac{\overline{q}}{2\pi\, ca^2}, \tag{18}$$

then Eq. (17) may be written as

$$\Theta = F + \frac{1}{2}\left(1 - n^2\right) \left(1 + \frac{\varphi^2}{2}\right) \tag{19}$$

where

$$F = \int_{r_1}^{r_2} r w dr. \tag{20}$$

Substituting from Eq. (10) in Eq. (20) yields

$$\frac{dP}{dz} = \frac{4F + 2\left(1 - n^2\right) r_2^2}{\frac{[I_1(r_2) - I_1(r_1)]^2}{I_2(r_2) - I_2(r_1)} - I_3}, \tag{21}$$

where

$$I_3 = \int_{r_1}^{r_2} \frac{r^3}{\mu\,(r)} dr. \tag{22}$$

The pressure rising ΔP_λ and drag (friction) forces $F_\lambda^{(i)}$ and $F_\lambda^{(o)}$ (at the walls) in the two peristaltic tubes of length λ, in the dimensionless form, are given by

$$\Delta P_\lambda = \int_0^1 \left(\frac{dP}{dz}\right) dz, \tag{23}$$

$$F_\lambda^{(i)} = \int_0^1 r_1^2 \left(-\frac{dP}{dz}\right) dz, \tag{24}$$

$$F_\lambda^{(o)} = \int_0^1 r_2^2 \left(-\frac{dP}{dz}\right) dz. \tag{25}$$

The influence of viscosity variation through the gap between two coaxial peristaltic tubes can be shown in Eqs. (23)-(25) to give a function of viscosity $\mu\,(r)$. For the present implementation, we assume that the viscosity variation in non-dimensional form as mentioned by Srivastava *et al.* [7] as:

$$\mu\,(r) = e^{-\alpha r}, \tag{26}$$

or

$$\mu\,(r) = 1 - \alpha r \quad for\ \alpha \ll 1. \tag{27}$$

Here α is a viscosity parameter.

This assumption was justified physiologically as shown in reference [10].

By substituting from Eq. (27) in Eqs. (11), (12), (22), using $r_1 = n\, r_2$ and Eq. (21), we obtain

$$\frac{dP}{dz} = \frac{c_1}{r_2^4} + \frac{c_2}{r_2^2} - c_3 \left(\frac{c_1}{r_2^3} + \frac{c_2}{r_2}\right), \tag{28}$$

where

$$c_1 = \frac{16F}{k_2}, \quad c_2 = \frac{8k_1}{k_2}, \; c_3 = -4\alpha k_3, \tag{29a}$$

$$k_1 = 1 - n^2, \quad k_2 = n^4 - \frac{k_1^2}{\log\,(n)} - 1, \tag{29b}$$

$$k_3 = \frac{k_1^2\,(1-n)}{4k_2\,(\log\,(n))^2} + \frac{k_1\left(1-n^3\right)}{3k_2 \log\,(n)} + \frac{1-n^5}{5k_2}. \tag{29c}$$

Substituting from Eq. (28) in Eqs. (23-25) yields

$$\Delta P_\lambda = c_1\, J_4 + c_2\, J_2 - c_3\,(c_1\, J_3 + c_2\, J_1)\,, \tag{30}$$

$$F_\lambda^{(i)} = -n^2\,[c_1\, J_2 + c_2 - c_3\,(c_1\, J_1 + c_2)]\,, \tag{31}$$

$$F_\lambda^{(o)} = -c_1\, J_2 - c_2 + c_3\,(c_1\, J_1 + c_2)\,, \tag{32}$$

where

$$J_1 = \frac{1}{\left(1-\varphi^2\right)^{1/2}}, \quad J_2 = \frac{1}{\left(1-\varphi^2\right)^{3/2}},$$
$$J_3 = \frac{2+\varphi^2}{2\left(1-\varphi^2\right)^{5/2}}, \quad J_4 = \frac{2+3\,\varphi^2}{2\left(1-\varphi^2\right)^{7/2}}. \tag{33}$$

Substituting from Eqs. (29) and (33) using (19) in Eqs. (30-32) yields (34)–(36), as shown at the bottom of the next page. Taking the limit as $n \to 0$ (i.e., in absence of the peristaltic endoscope), the results that are obtained in Eqs. (34-36) reduce to

$$\Delta P_\lambda = -2\left[\frac{8\Theta + 4\varphi^2\,(3\Theta - 4) + \varphi^4}{\left(1-\varphi^2\right)^{7/2}}\right] + 8\alpha\left[\frac{8\Theta + 4\varphi^2\,(\Theta - 3) + 3\varphi^4}{5\left(1-\varphi^2\right)^{5/2}}\right], \tag{37}$$

$$F_\lambda^{(o)} = 8 - \frac{4\left(2 - 4\Theta + \varphi^2\right)}{\left(1-\varphi^2\right)^{3/2}} + \frac{16\alpha}{5}\left(\frac{2 - 4\Theta + \varphi^2}{\left(1-\varphi^2\right)^{1/2}} - 2\right) \tag{38}$$

which are the same results obtained by Shapiro *et al.* [6] and Srivastava [14] in absence of the viscosity parameter α. Also, these results are derived by Shukla *et al.* [5] in absence of the peripheral layer.

$$w\,(r,z) = \frac{1}{2}\frac{dP}{dz}\left[I_1\,(r) - \frac{I_2\,(r)\,[I_1\,(r_2) - I_1\,(r_1)] + I_1\,(r_1)\,I_2\,(r_2) - I_1\,(r_2)\,I_2\,(r_1)}{I_2\,(r_2) - I_2\,(r_1)}\right] - 1, \tag{10}$$

III. TRAPPING AT THE CENTERLINE OF THE GAP

Trapping phenomenon was studied by several investigators as shown in literature [4], [6], [19]–[21]. Following Siddiqui and Schwarz [22], the trapping limits have been determined as $\frac{\Theta_{\min}}{\Theta_{\max}}$ is a function of occlusion φ, where $\Theta_{\min}$ is the minimum flow rate and $\Theta_{\max}$ is the maximum flow rate. The minimum flow rate is obtained by Eqs. (10), (19) and (28) when $w = 0$ at $r = \left(k_4\, r_2^2 + \alpha\, k_5\, r_2^3\right)^{1/2}$, where $k_4 = -k_1/2\,\log(n)$ and $k_5 = -k_1\,(1-n)/2\,(\log(n))^2 + \left(n^3-1\right)/3\log(n)$ and solving it with respect to Θ, then we get

$$\Theta_{\min} = -\frac{k_1\phi\,(4+\phi)}{4} + \frac{k_2\log(n)\,(1+\phi)^2}{2k_1\log(k_4)+4\,(k_4-1)\log(n)} + \alpha\,(k_6+k_7+k_8)\,(1+\phi)^3 \tag{39}$$

where k_6, k_7, k_8, as shown at the bottom of the page. The maximum flow rate has been obtained by setting $\Delta P_\lambda = 0$ in Eq. (34) and solving it with respect to Θ, then we get

$$\Theta_{\max} = \frac{k_1\,\varphi^2\left(16-\varphi^2\right)}{4\left(2+3\,\varphi^2\right)} - \frac{8\,\alpha\,k_1\,k_3\,\varphi^2\,\left(1-\varphi^2\right)^3}{\left(2+3\varphi^2\right)^2}, \tag{40}$$

and hence the flow rate ratio $\Theta_{\min}/\Theta_{\max}$, neglecting the terms of order α^2, reduces to (41), as shown at the bottom of the page, where

$$\begin{aligned} k_{10} &= k_6 + k_7 + k_8 \\ k_{11} &= -k_1\varphi\,(4+\varphi)/4 + k_2\,(1+\varphi)^2\log(n)\Big/k_9, \\ k_9 &= 2\,k_1\log(k_4) + 4\,(k_4-1)\log(n) \end{aligned}$$

By taking the limit of minimum and maximum flow rate ratio $\Theta_{\min}/\Theta_{\max}$ as n tends to zero, one obtains the following form (42), as shown at the bottom of the next page. This result is the same as given by Shapiro *et al.* [6] as $\alpha = 0$.

Physically, minimum and maximum flow rate must be real and satisfy the inequality $0 \le \Theta_{\min} \le \Theta_{\max}$. So, trapping takes place such that $0 \le \Theta_{\min}/\Theta_{\max} \le 1$ for all values of radius ratio n and amplitude ratio φ. The boundary of the trapping region has been obtained by calculating minimum and maximum flow rate ratio $\Theta_{\min}/\Theta_{\max}$ for different values of the parameter φ at $n = 0,\ 0.32$.

$$\begin{aligned} \Delta P_\lambda &= 8\left[\left(\Theta - \frac{k_1\left(2+\varphi^2\right)}{4}\right)\left(2+3\varphi^2\right) + k_1\left(1-\varphi^2\right)^2\right]\Big/ k_2\left(1-\varphi^2\right)^{7/2} \\ &\quad +32\alpha k_3\left[\left(\Theta - \frac{k_1\left(2+\varphi^2\right)}{4}\right)\left(2+\varphi^2\right) + k_1\left(1-\varphi^2\right)^2\right]\Big/ k_2\left(1-\varphi^2\right)^{5/2}, \end{aligned} \tag{34}$$

$$\begin{aligned} F_\lambda^{(i)} &= -8n^2\left[2\Theta - \frac{k_1\left(2+\varphi^2\right)}{2} + k_1\left(\left(1-\varphi^2\right)^{3/2}\right)\right]\Big/ k_2\left(1-\varphi^2\right)^{3/2} \\ &\quad - 32\alpha k_3 n^2\left[2\Theta - \frac{k_1\left(2+\varphi^2\right)}{2} + k_1\left(1-\varphi^2\right)^{1/2}\right]\Big/ k_2\left(1-\varphi^2\right)^{1/2}, \end{aligned} \tag{35}$$

$$\begin{aligned} F_\lambda^{(o)} &= -8\left[2\Theta - \frac{k_1\left(2+\varphi^2\right)}{2} + k_1\left(1-\varphi^2\right)^{3/2}\right]\Big/ k_2\left(1-\varphi^2\right)^{3/2} \\ &\quad -32\alpha k_3\left[2\Theta - \frac{k_1\left(2+\varphi^2\right)}{2} + k_1\left(1-\varphi^2\right)^{1/2}\right]\Big/ k_2\left(1-\varphi^2\right)^{1/2}. \end{aligned} \tag{36}$$

$$\begin{aligned} k_6 &= \frac{k_1 k_2\,(n-1)\log(k_4)}{2\,(k_1\log(k_4)+2\,(k_4-1)\log(n))^2} \\ k_7 &= \frac{k_2\log(n)\left(-3k_1\left(-2k_4+2k_4^{3/2}+k_5\right)+2k_4\left(-1+n^3+6k_3\left(n^2-1\right)\right)\log(k_4)\right)}{6k_4\,(k_1\log(k_4)+2\,(k_4-1)\log(n))^2} \\ k_8 &= -\frac{k_2\,(\log(n))^2\left(-2+12k_3\,(k_4-1)+2k_4^{3/2}+3k_5\right)}{3\,(k_1\log(k_4)+2\,(k_4-1)\log(n))^2} \end{aligned}$$

$$\frac{\Theta_{\min}}{\Theta_{\max}} = -\frac{4\left(2+3\,\varphi^2\right)k_{11}}{k_1\,\varphi^2\left(\varphi^2-16\right)} + \frac{4\,\alpha\left(-k_{10}\,(1+\varphi)^3\left(\varphi^2-16\right)\left(2+3\,\varphi^2\right) - 32\,k_3\left(\varphi^2-1\right)^3\,k_{11}\right)}{k_1\,\varphi^2\left(\varphi^2-16\right)^2}, \tag{41}$$

IV. SEPARATED FLOW (TRAPPING AT THE BOUNDARY OF THE GAP)

To predict separated flow at the boundary, the magnitude of the vorticity vector equals to zero at the boundary, i.e.,

$$\zeta = \frac{\partial u}{\partial z} - \frac{\partial w}{\partial r} = 0 \text{ at } r = r_2,\ r = r_1 \tag{43}$$

By substituting from Eqs. (11), (12) and (28) in Eq. (10) and making use of Eq. (27), we get the axial velocity of the fluid as:

$$\begin{aligned} w = {} & d_1 \frac{r^3 r_2'}{r_2^5} + \left(-d_1 r + d_2 \frac{r^3}{2} + d_3 r \log(\frac{r}{r_2})\right) \\ & \times \left(\frac{r_2'}{r_2^3}\right) + d_4 \frac{r\, r_2'}{2\, r_2\, 2} - \left(\frac{r^2}{r_2^4}\right) \\ & + \alpha \left\{ d_5 \frac{r^3}{r_2^4} + d_6 \frac{r^2}{r_2^3} + d_7 \frac{r}{r_2^2} - \frac{d_8}{r_2} \right. \\ & - \frac{d_9}{r_2} \log\left(\frac{r}{r_2}\right) + d_{10} \frac{r^3}{r_2^2} + d_{11} \frac{r^2}{r_2} \\ & \left. + d_{12}\, r - d_{13}\, r_2 - d_{14}\, r_2 \log\left(\frac{r}{r_2}\right) \right\}, \end{aligned} \tag{44}$$

where the prime means differentiation with respect to z.

To obtain the radial velocity of the fluid, we substitute from Eq. (44) into Eq. (5) using the boundary condition (8b), we have the radial velocity of the fluid in the following form:

$$\begin{aligned} u = {} & d_1 r^3 \frac{r_2'}{r_2^5} + \left(-d_1 r + \frac{d_2}{2} r^3 + d_3 r \log(\frac{r}{r_2})\right) \left(\frac{r_2'}{r_2^3}\right) \\ & + \frac{d_4}{2} \left(\frac{r r_2'}{r_2}\right) - (2 + d_2 + d_4) \left(\frac{r_2 r_2'}{2r}\right) \\ & + \alpha \left\{ \left(\left(-\frac{4}{5} d_5 + \frac{1}{12} (-9d_6 - 8d_7 + 6d_8 + 3d_9) \right) \frac{1}{r} \right. \right. \\ & \left. \left. + \frac{1}{4} r \left(2d_{13} - 3d_{14} + 2d_{14} \log(\frac{r}{r_2})\right) \right) r_2' \right. \\ & \left. + \frac{4}{5} d_5 \frac{r^4 r_2'}{r_2^5} + \frac{3}{4} d_6 \frac{r^3 r_2'}{r_2^4} + \frac{\left(\frac{2}{3} d_7 r^2 + \frac{2}{5} d_{10} r^4\right) r_2'}{r_2^3} \right. \\ & \left. + \frac{r \left(-2d_8 - d_9 + d_{11} r^2 - 2d_9 \log(\frac{r}{r_2})\right) r_2'}{4 r_2^2} \right. \\ & \left. - \frac{(8d_{10} + 5\,(d_{11} + 2d_{13} - 3d_{14}))\, r_2^2 r_2'}{20r} \right\}, \end{aligned} \tag{45}$$

where $d_1 - d_{14}$, as shown at the bottom of the page. Substituting from Eqs. (44) and (45) into Eq. (43), we get

$$\begin{aligned} & r_2^3 r_2'' + (2d_2 + d_4 + 1)\, r_2^2 r_2'^2 + (2d_1 + d_3)\, r_2'^2 \\ & + (2d_2 + d_4)\, r_2^2 + 2d_1 + d_3 + \alpha\, [(2d_{10} + d_{11} + d_{13} \\ & - d_{14})\, r_2^3 r_2'^2 + (4d_5 + 3d_6 + 2d_7 - d_8 - d_9)\, r_2 r_2'^2 \\ & + (3d_{10} + 2d_{11} + d_{12} - d_{14})\, r_2^3 + (3d_5 + 2d_6 \\ & + d_7 - d_9)\, r_2] = 0, \end{aligned} \tag{46}$$

$$\begin{aligned} & r_1^3 r_1'' + (2d_2 + d_4 + 1)\, r_1^2 r_1'^2 + (2d_1 + d_3)\, r_1'^2 \\ & + (2d_2 + d_4)\, r_1^2 + 2d_1 + d_3 + \alpha\, [(2d_{10} + d_{11} + d_{13} \\ & - d_{14})\, r_1^3 r_1'^2 + (4d_5 + 3d_6 + 2d_7 - d_8 - d_9)\, r_1 r_1'^2 \\ & + (3d_{10} + 2d_{11} + d_{12} - d_{14})\, r_1^3 \\ & + (3d_5 + 2d_6 + d_7 - d_9)\, r_1] = 0. \end{aligned} \tag{47}$$

Substituting from Eq. (9) in Eqs. (46) and (47), we have (48) and (49), as shown at the bottom of the next page. Since separated flow occurs on the boundaries that are functions of z, then we must find z as a function of parameters that are including parameters of both the peristaltic motion of the walls and viscous flow in the thin annuli. Thus by substituting from Eq. (19) in Eqs. (48) and (49) and then solve them numerically. Hence, we obtain the axial component of separated flow points z_s on the outer and inner peristaltic tubes respectively as a function of parameters α, φ, n and Θ.

V. NUMERICAL RESULTS AND DISCUSSION

For discussion our results, we calculate the non-dimensional pressure rising ΔP_λ, and drag (friction) forces (at the walls) in the two peristaltic tubes for various given values of the non-dimensional time-mean flow Θ, occlusion ϕ, and radius ratio n. As shown in Srivastava and Srivastava [23], one uses the values of various parameters as: $a_2 = 1.25\,cm$.

$$\frac{\Theta_{\min}}{\Theta_{\max}} = \frac{(1 - 2\varphi)\left(2 + 3\varphi^2\right)}{\varphi^2\left(16 - \varphi^2\right)} - \frac{2\alpha\,(1 + \varphi)^3\left(99\,\varphi^4 - 336\,\varphi^3 + 386\,\varphi^2 - 240\,\varphi + 16\right)}{15\,\varphi^2\left(16 - \varphi^2\right)^2}. \tag{42}$$

$$d_1 = \frac{c_1}{4}, d_2 = \frac{c_2}{4}, \quad d_3 = \frac{c_1\left(1 - n^2\right)}{4\log(n)},\ d_4 = \frac{c_2\left(1 - n^2\right)}{4\log(n)},\ d_5 = \frac{c_1}{6},\ d_6 = c_1 k_3,\ d_7 = \frac{c_1\left(1 - n^2\right)}{4\log(n)}$$

$$d_8 = \frac{c_1\left(3 - 3n^2 + 2\,(1 + 6k_3)\log(n)\right)}{12\log(n)}, \quad d_9 = \frac{c_1\,(n-1)\left(3 - 3n^2 + 2\left(1 + n + n^2 + 6k_3(1 + n)\right)\log(n)\right)}{12\,(\log(n))^2},$$

$$d_{10} = \frac{c_2}{6}, d_{11} = c_2 k_3, \quad d_{12} = \frac{c_2\left(1 - n^2\right)}{4\log(n)},\ d_{13} = \frac{c_2\left(3 - 3n^2 + 2\,(1 + 6k_3)\log(n)\right)}{12\log(n)},$$

$$d_{14} = \frac{c_2\,(n-1)\left(3 - 3n^2 + 2\left(1 + n + n^2 + 6k_3(1 + n)\right)\log(n)\right)}{12\,(\log(n))^2}.$$

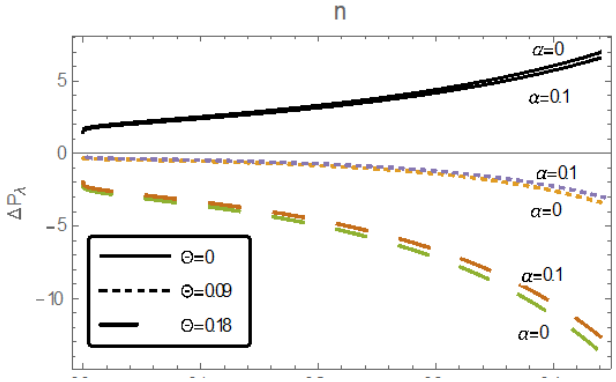

FIGURE 2. The pressure rise against radius ratio at $\varphi = 0.2$.

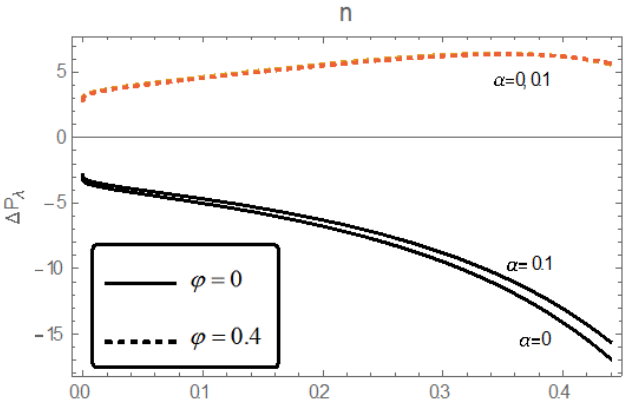

FIGURE 3. The pressure rise against radius ratio at $\Theta = 0.18$.

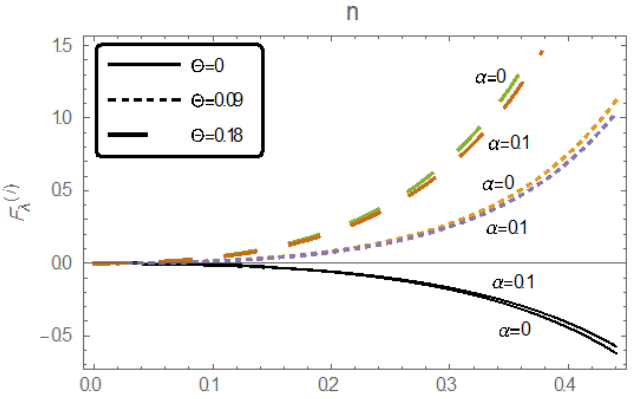

FIGURE 4. The friction force on inner peristaltic tube against radius ratio at $\varphi = 0.2$.

$\lambda = 8.01\,cm.$, $c = 2cm./\min$. The parameter of viscosity α takes the values 0 and 0.1, as reported in Srivastava *et al.* [7]. Since the radius of the small intestine, $a_2 = 1.25\,cm.$, is small compared with the wavelength $\lambda = 8.01\,cm.$, then the theory of long wavelength and creeping flow of the present implementing remains usable. Also, Lew *et al.* [24] observed that Reynolds number in the small intestine was very small. Cotton and Williams [25] reported diameter of gastrointestinal rigid endoscopes are among 8 and 11 mm. Besides, Srivastava and Srivastava [23] reported the radius of the small intestine is 1.25 $cm.$, then the maximum value of the radius ratio n for rigid endoscopes becomes 0.44, but the radius ratio n for peristaltic endoscopes takes the values greater than zero or less than one. Equations (34), (35) and (36) are drawn in Figs. 2-7 respectively. Whereas, Eq (41) is drawn in Fig. 8.

Figs. 2 and 3 perform the pressure rise variation ΔP_λ against radius ratio n at $\varphi = 0.2$ and $\Theta = 0.18$ respectively, which show that the magnitude of pressure rising increases when radius ratio n increases for various values of flow rate Θ. Since increasing radius ratio means that the volume flow rate decreases, then the pressure rise increases. Physically, decreasing of the volume flow rate means that the velocity field decreases. Hence, the pressure rise increases. But increasing viscosity parameter α decreases the pressure rise because the increasing viscosity parameter means that fluid viscosity decreases. Furthermore, there is approximately no variation of pressure rise with viscosity parameter α at $\varphi = 0.2, \Theta = 0.09$ and $\varphi = 0.4, \Theta = 0.18$ as shown in Figs. 2 and 3 respectively. Also, augmented pumping, where $\Theta > 0$ and $\Delta P_\lambda < 0$ (favorable pressure gradient), takes place at

$$
\begin{aligned}
&-4\pi^2\varphi\sin(2\pi z)(1+\varphi\sin(2\pi z))^3+4\pi^2\varphi^2\cos^2(2\pi z)(1+\varphi\sin(2\pi z))^2(2d_2+d_4+1)\\
&\quad+4\pi^2\varphi^2\cos^2(2\pi z)(2d_1+d_3)+(2d_2+d_4)(1+\varphi\sin(2\pi z))^2+2d_1+d_3\\
&\quad+\alpha\Big[4\pi^2\varphi^2\cos^2(2\pi z)(1+\varphi\sin(2\pi z))^3(2d_{10}+d_{11}+d_{13}-d_{14})\\
&\quad+4\pi^2\varphi^2\cos^2(2\pi z)(1+\varphi\sin(2\pi z))(4d_5+3d_6+2d_7-d_8-d_9)\\
&\quad+(1+\varphi\sin(2\pi z))^3(3d_{10}+2d_{11}+d_{12}-d_{14})+(1+\varphi\sin(2\pi z))(3d_5+2d_6+d_7-d_9)\Big]=0, \qquad (48)\\
&-4\pi^2\varphi\sin(2\pi z)(1+\varphi\sin(2\pi z))^3+4\pi^2\varphi^2\cos^2(2\pi z)(1+\varphi\sin(2\pi z))^2(2d_2+d_4+1)\\
&\quad+4\pi^2\varphi^2\cos^2(2\pi z)(2d_1+d_3)+(2d_2+d_4)(1+\varphi\sin(2\pi z))^2+2d_1+d_3\\
&\quad+\alpha\Big[4\pi^2\varphi^2\cos^2(2\pi z)(1+\varphi\sin(2\pi z))^3(2d_{10}+d_{11}+d_{13}-d_{14})\\
&\quad+4\pi^2\varphi^2\cos^2(2\pi z)(1+\varphi\sin(2\pi z))(4d_5+3d_6+2d_7-d_8-d_9)\\
&\quad+(1+\varphi\sin(2\pi z))^3(3d_{10}+2d_{11}+d_{12}-d_{14})+(1+\varphi\sin(2\pi z))(3d_5+2d_6+d_7-d_9)\Big]=0, \qquad (49)
\end{aligned}
$$

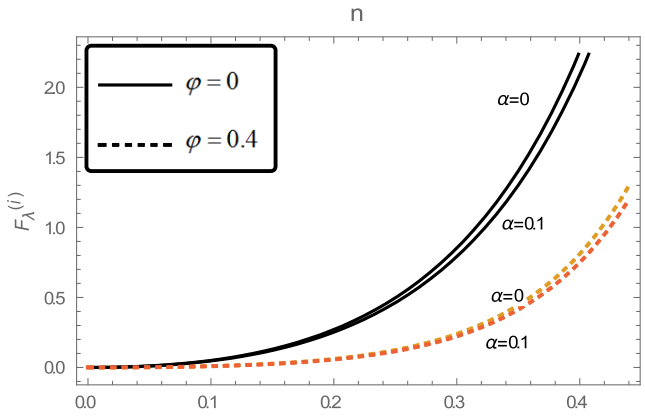

FIGURE 5. The friction force on inner peristaltic tube against radius ratio at $\Theta = 0.18$.

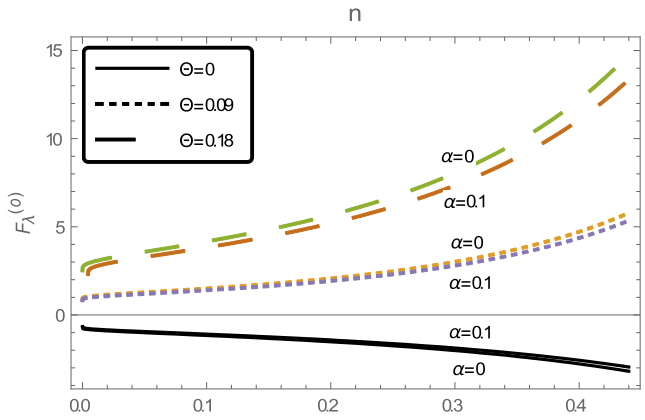

FIGURE 6. The friction force on outer peristaltic tube against radius ratio at $\varphi = 0.2$.

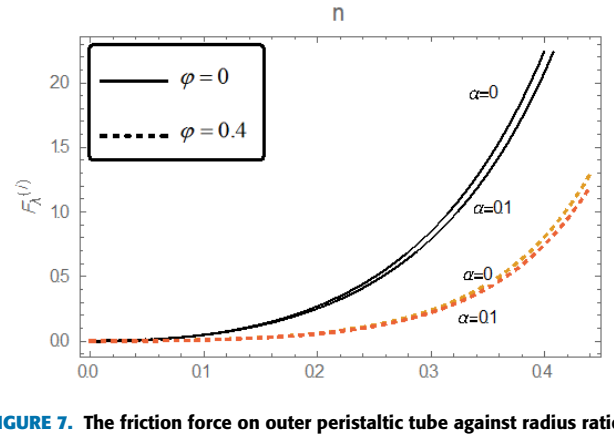

FIGURE 7. The friction force on outer peristaltic tube against radius ratio at $\Theta = 0.18$.

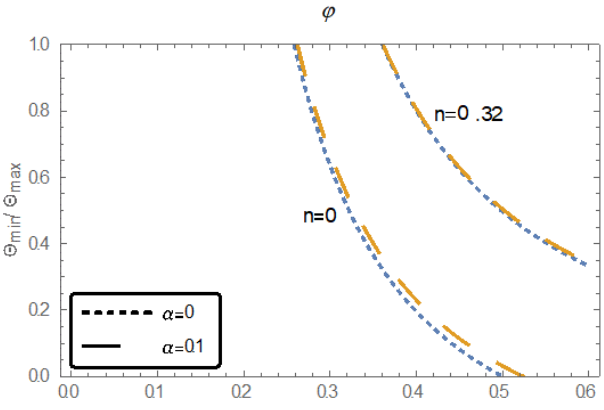

FIGURE 8. Graph of $\Theta_{min}/\Theta_{max}$ against amplitude ratio φ.

$\varphi = 0$ (no peristalsis), but peristaltic pumping, where $\Theta > 0$ and $\Delta P_\lambda > 0$ (adverse pressure gradient), takes place at $\varphi = 0.4$ as shown in Fig. 3.

Experimental results in vivo pig had been obtained by Grundfest *et al.* [26] showed that the intestinal diameter increases with increasing intraluminal intestinal pressure in presence of a robotic endoscope and this agrees with our theoretical results which state that the pressure rising increases when radius ratio increases. Physically, increasing the radius ratio implies increasing of the intestinal diameter.

Figs. 4-7 represent the variation of drag (friction) forces on a peristaltic endoscope and on a peristaltic tube $F_\lambda^{(i)}$ and $F_\lambda^{(o)}$ respectively with radius ratio n at amplitude ratio $\varphi = 0.2$ and time-mean flow $\Theta = 0.18$. That shows the magnitude of drag (friction) forces on the peristaltic endoscope and on the peristaltic tube increase when radius ratio n increases for various values Θ and α, but they decrease when viscosity parameter α increases at $\varphi = 0$, 0.4 for various values of radius ratio n. Similarly, there is approximately no variation of drag (friction) forces on the peristaltic endoscope and the peristaltic tube with viscosity parameter α at $\varphi = 0.2$, $\Theta = 0$ as shown in Figs.4 and 6. Moreover, reflux (backward flow), where $\Theta > 0$, $F_\lambda^{(i)} > 0$ and $F_\lambda^{(o)} > 0$, takes place at $\Theta = 0.09$, 0.18 for various values of radius ratio when viscosity parameter $\alpha = 0$, 0.1 and $\varphi = 0.2$, 0.4. Furthermore, drag (friction) force on the peristaltic endoscope is smaller than that on the outer peristaltic tube. This happens because amplitude ratio ϕ on the outer peristaltic tube is greater than that on the peristaltic endoscope.

The next results in tables 1 and 2 for the pressure rise ΔP_λ and friction forces $F_\lambda^{(i)}$ and $F_\lambda^{(o)}$ of a rigid endoscope and a peristaltic endoscope have been obtained from equations (2.35-2.37) in reference [10] and equations (34-36) in the present study.

It is obvious from tables 1 and 2 that the absolute values of pressure rising and friction forces in presence of rigid endoscope are smaller than the corresponding values in presence of a peristaltic endoscope at $0.1 \leq \varphi \leq 0.2$, but they are greater at $0.3 \leq \varphi \leq 0.6$ for the fluid with constant and variable viscosity.

Fig. 8 shows that the trapping limit, for fluids of a constant viscosity ($\alpha = 0$) and that of a variable viscosity ($\alpha = 0.1$), takes place at $0.26 \leq \varphi < 0.5$ and $0.27 \leq \varphi \leq 0.52$ for $\alpha = 0$, 0.1 respectively when $n = 0$ (absence of the peristaltic endoscope), but it takes place at $0.36 \leq \varphi \leq 0.6$ when $n = 0.32$ (presence of the peristaltic endoscope). Also, it is clear that the trapping limit increases when viscosity parameter α increases in absence of the inner peristaltic tube, but it is independent of viscosity parameter in presence of

TABLE 1. The pressure rise and friction forces in presence of a rigid endoscope at $\Theta = 0.09$ and $n = 0.32$.

φ	ΔP_λ		$F_\lambda^{(i)}$		$F_\lambda^{(o)}$	
	$\alpha = 0$	$\alpha = 0.1$	$\alpha = 0$	$\alpha = 0.1$	$\alpha = 0$	$\alpha = 0.1$
0.1	-3.89585	-3.68174	0.415138	0.377736	4.36853	4.03491
0.2	0.361751	0.407488	-0.0385036	-0.0473769	1.7779	1.63082
0.3	12.8635	12.25	-1.33875	-1.26282	-4.07475	-4.12444
0.4	53.6377	50.6017	-5.51668	-5.18815	-19.1344	-17.8374
0.5	238.385	234.258	-24.7609	-23.6663	-66.0309	-63.4274
0.6	2509.61	2421.19	-259.768	-251.856	-447.503	-433.187

TABLE 2. The pressure rise and friction forces in presence of a peristaltic endoscope at $\Theta = 0.09$ and $n = 0.32$.

φ	ΔP_λ		$F_\lambda^{(i)}$		$F_\lambda^{(o)}$	
	$\alpha = 0$	$\alpha = 0.1$	$\alpha = 0$	$\alpha = 0.1$	$\alpha = 0$	$\alpha = 0.1$
0.1	-4.30774	-3.98554	0.47728	0.44138	4.66094	4.31035
0.2	-1.55357	-1.37971	0.335314	0.304634	3.27455	2.97495
0.3	4.61107	4.48506	0.0708406	0.0493248	0.691803	0.481688
0.4	18.0172	17.3258	-0.370627	-0.378206	-3.6194	-3.69342
0.5	49.3158	47.521	-1.10213	-1.08947	-10.7629	-10.6394
0.6	133.215	129.046	-2.37714	-2.33508	-23.2142	-22.8035

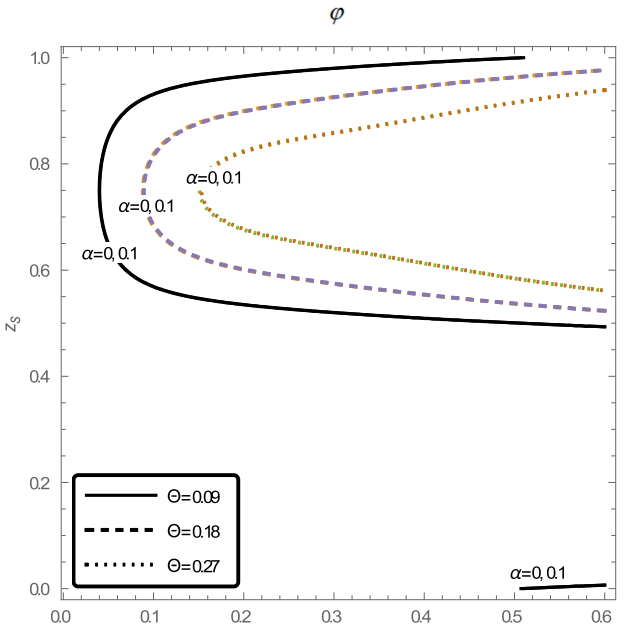

FIGURE 10. The axial component of separated flow points on outer peristaltic tube against amplitude ratio at $n = 0.44$.

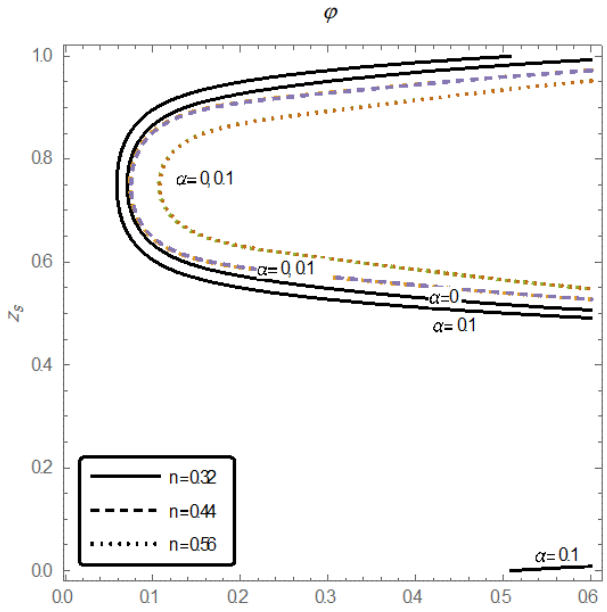

FIGURE 9. The axial component of separated flow points on outer peristaltic tube against amplitude ratio at $\Theta = 0.18$.

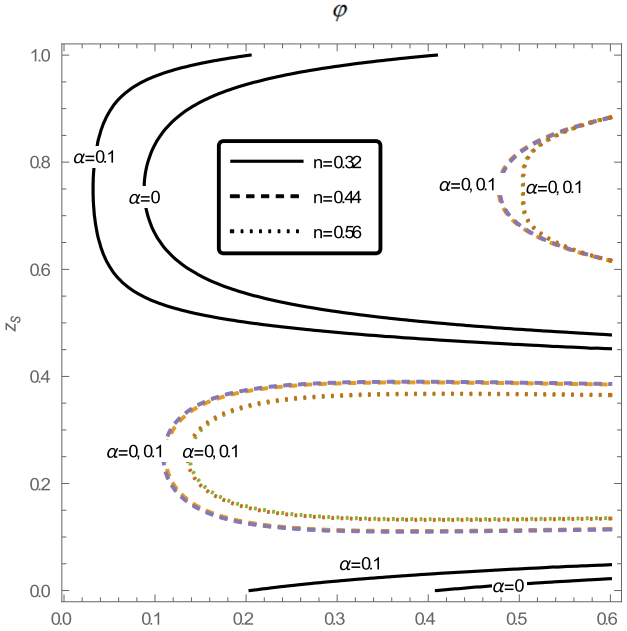

FIGURE 11. The axial component of separated flow points on inner peristaltic tube against amplitude ratio at $\Theta = 0.18$.

the peristaltic endoscope. Moreover, the trapping limit, which was obtained by Shapiro *et al.* [6], agrees with our results when $n = 0$ and $\alpha = 0$.

To discuss the phenomenon of separated flow (trapping) at walls bounded the gap between the peristaltic endoscope and the small intestine. We calculate numerically the axial component of separated flow points on the outer peristaltic tube wall and on the inner peristaltic tube wall from Eqs. (48) and (49) respectively. Equations (48) and (49) are drawn in Figs. 9-12 respectively.

Figs. 9-12 show the relation between axial component z_s of separated flow points on the outer and inner peristaltic tubes walls and occlusion φ. We notice from Figs.9-12 at certain values of radius ratio n, amplitude ratio φ, volume flow rate Θ and viscosity parameter Θ that the axial component z_s of separated flow points on the outer and inner peristaltic tubes walls bifurcates into two branches. For the outer peristaltic tube, one of them (upper branch) approaches to outlet of contraction region and the other (lower branch) approaches

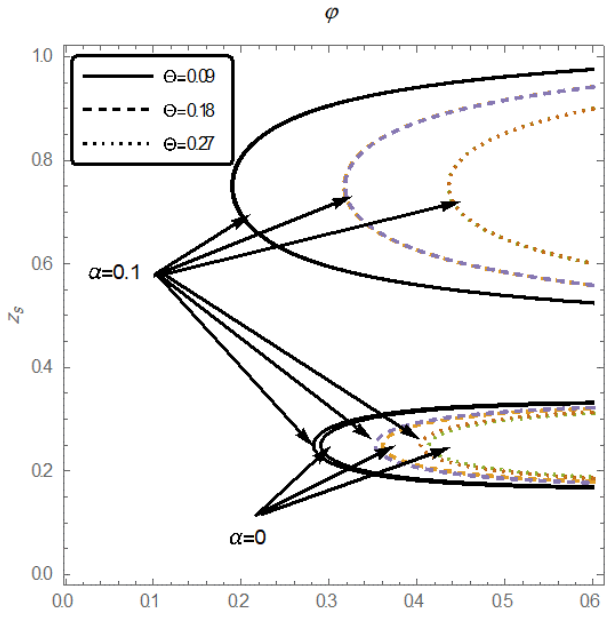

FIGURE 12. The axial component of separated flow points on inner peristaltic tube against amplitude ratio at $n = 0.44$.

to inlet of contraction region. But for the inner peristaltic tube, bifurcation of the axial component z_s of separated flow points takes place in relaxation and contraction regions. Physically, this means that the streamlines under certain conditions divide to trap a fluid which totally moving with the same speed of the peristaltic wave. Also, it is evident from Figs. 9-12 that the axial component of separated flow points on the peristaltic endoscope wall and on the small intestine wall is approximately independent of viscosity parameter at $\{n = 0.44,\ 0.56,\ \Theta = 0.09,\ 0.18,\ 0.27\}$. In addition, the trapping limit increases when radius ratio and volume flow rate increase. Moreover, Figs. 9 and 10 declare that trapping region on the outer peristaltic tube takes place in a contraction region for different values of radius ratio and volume flow rate, but it takes place in relaxation region only at $\{n = 0.32,\ \varphi = 0.51,\ \alpha = 0.1,\ \Theta = 0.18\}$ and $\{n = 0.44,\ \varphi = 0.51,\ \alpha = 0.1,\ \Theta = 0.18\}$. Furthermore, Figs. 11 and 12 show that trapping region on the inner peristaltic tube takes place in contraction and relaxation regions for different values of radius ratio and volume flow rate, but it takes place in relaxation region only at $\{n = 0.44,\ \alpha = 0,\ \Theta = 0.09,\ 0.18,\ 0.27\}$. It is clear from Figs. 9-12 that there are fixed points (critical amplitude ratios) which interchange their stability with other fixed points as the parameters α, n and Θ are varied. So, there are bifurcations of a flow between coaxial peristaltic tubes. This phenomenon occurs as a result of sequences of relaxations and contractions of coaxial peristaltic tubes.

VI. CONCLUSION

As a result of previous analyses, we conclude that the flow field of a fluid with constant density and viscosity variation through a gap between two coaxial peristaltic tubes is remarkable.

More exactly:

- The peristaltic endoscope is more appropriate than the rigid endoscope for peristaltic organs whose amplitude ratios are 0.3, 0.4, 0.5 and 0.6, but the rigid endoscope is more appropriate than the peristaltic endoscope for peristaltic organs whose amplitude ratios are 0.1 and 0.2.
- Increasing radius ratio increases the pressure rise in the peristaltic pumping and augmented pumping regions.
- The friction forces increase with increasing radius ratio in peristaltic pumping and reflux regions.
- The trapping limit on the centerline of the gap between coaxial peristaltic tubes is independent of viscosity parameter in presence of the peristaltic endoscope ($n = 0.32$), but it increments with increasing viscosity parameter in absence of the peristaltic endoscope ($n = 0$) .
- The separated limit on the boundary increments with increasing radius ratio and volume flow rate, but it declines when viscosity parameter increases.
- Separated flow occurs at the surfaces of peristaltic movement.
- The present mathematical model of a peristaltic endoscope is considered as benchmark research for endoscopes' development.

REFERENCES

[1] E. V. Mangan, D. A. Kingsley, R. D. Quinn, and H. J. Chiel, "Development of a peristaltic endoscope," in *Proc. IEEE Int. Conf. Robot. Autom.*, Washington, DC, USA, May 2002, pp. 347–352.
[2] T. Nakamura, Y. Hidaka, M. Yokojima, and K. Adachi, "Development of peristaltic crawling robot with artificial rubber muscles attached to large intestine endoscope," *Adv. Robot.*, vol. 26, no. 10, pp. 1161–1182, Jul. 2012.
[3] R. Roos and P. S. Lykoudis, "The fluid mechanics of the ureter with an inserted catheter," *J. Fluid Mech.*, vol. 46, pp. 625–630, Apr. 1971.
[4] R. R. Adabala and U. Srinivasan, "Peristaltic pumping in a circular tube in the presence of an eccentric catheter," *J. Biomechanical Eng.*, vol. 117, no. 4, pp. 448–454, Nov. 1995.
[5] J. B. Shukla, R. S. Parihar, R. P. Rao, and S. P. Gupta, "Effects of peripheral-layer viscosity on peristaltic transport of a bio-fluid," *J. Fluid Mech.*, vol. 97, pp. 225–237, Mar. 1980.
[6] A. H. Shapiro, M. Y. Jaffrin, and S. L. Weinberg, "Peristaltic pumping with long wave lengths at low Reynolds number," *J. Fluid Mech.*, vol. 37, pp. 799–825, Jul. 1969.
[7] L. M. Srivastava, V. P. Srivastava, and S. N. Sinha, "Peristaltic transport of a physiological fluid part I Flow in non-uniform geometry," *Biorheology*, vol. 20, pp. 153–166, 1983.
[8] A. E. H. A. Naby, A. E. Misiery, and I. I. Shamy, "Hydromagnetic flow of fluid with variable viscosity in uniform tube with peristalsis," *J. Phys. A, Math. Gen.*, vol. 36, pp. 8535–8547, Jul. 2003.
[9] A. E. H. Abd El Naby and A. E. M. El Misiery, "Effects of an endoscope and generalized Newtonian fluid on peristaltic motion," *Appl. Math. Comput.*, vol. 128, no. 1, pp. 19–35, May 2002.
[10] A. M. El Misiery, A. E. H. Abd EL Naby, and A. El Nagar, "Effects of a fluid with variable viscosity and an endoscope on peristaltic motion," *J. Phys. Soc. Jap.*, vol. 72, pp. 89–94, Jan. 2003.
[11] K. H. Mekheimer and S. Y. Abd elmaboud, "The influence of heat transfer and magnetic field on peristaltic transport of a Newtonian fluid in a vertical annulus: Application of an endoscope," *Phys. Lett. A*, vol. 372, pp. 1657–1665, Mar. 2008.
[12] T. Hayat, E. Momoniat, and M. F. Mahomed, "Endoscope effects on MHD peristaltic flow of a power-law fluid," *Math. Probl. Eng.*, vol. 2006, pp. 1–19, May 2006.

[13] T. Hayat, E. Momoniat, and M. F. Mahomed, "Peristaltic MHD flow of third grade fluid with an endoscope and variable viscosity," *J. Nonlinear Math. Phys.*, vol. 15, pp. 91–104, Aug. 2008.
[14] V. P. Srivastava, "Effects of an inserted endoscope on chyme movement in small intestine-A theoretical model," *AAM Int. J.*, vol. 2, pp. 79–91, Dec. 2007.
[15] H. Sadaf, M. U. Akbar, and S. Nadeem, "Induced magnetic field analysis for the peristaltic transport of non-Newtonian nanofluid in an annulus," *Int. J. Math. Comput. Simul.*, vol. 148, pp. 16–36, Jun. 2018.
[16] S. Akram, E. H. Aly, F. Afzal, and S. Nadeem, "Effect of the variable viscosity on the peristaltic flow of Newtonian fluid coated with magnetic field: Application of Adomian decomposition method for endoscope," *Coatings*, vol. 9, pp. 524–542, Aug. 2019.
[17] H. Rachid and M. T. Ouazzani, "Elctro-Magnetohydrodynamic peristaltic pumping of a biviscosity fluid between two coaxial deformable tubes through a porous medium," *Acta Phys. Pol. B*, vol. 48, pp. 1515–1527, Sep. 2017.
[18] L. B. McCash, S. Akhtar, S. Nadeem, S. Saleem, and A. Issakhov, "Viscous flow between two sinusoidally deforming curved concentric tubes: Advances in endoscopy," *Sci. Rep.*, vol. 11, Jul. 2021, Art. no. 15124.
[19] Y. C. Fung and C. S. Yih, "Peristaltic transport," *J. Appl. Mech.*, vol. 35, pp. 669–675, Dec. 1968.
[20] M. Y. Jaffrin, "Inertia and streamline curvature effects on peristaltic pumping," *Int. J. Eng. Sc.*, vol. 11, pp. 681–699, Jun. 1973.
[21] R. E. Abo-Elkhair, M. M. Bhatti, and S. Kh Mekheimer, "Magnetic force effects on peristaltic transport of hybrid bio-nanofluid (Au-Cu nanoparticles) with moderate Reynolds number: An expanding horizon," *Int. Commun. Heat Mass Transf.*, vol. 123, pp. 1–18. Mar. 2021.
[22] A. M. Siddiqui and W. H. Schwarz, "Peristaltic pumping of a third-order fluid in planar Channel," *J. Rhol. Acta*, vol. 32, pp. 47–56, Jan. 1993.
[23] L. M. Srivastava and V. P. Srivastava, "Peristaltic transport of a non-Newtonian fluid Applications to the vas defernes and small intestine," *Ann. Biomed. Eng.*, vol. 13, pp. 137–153, Mar. 1985.
[24] H. S. Lew, Y. C. Fung, and C. B. Lowenstein, "Peristaltic carrying and mixing of chyme," *J. Biomech.*, vol. 4, pp. 297–315, Jul. 1971.
[25] P. B. Cotton, and C. B. Williams, *Practical Gastrointestinal Endoscopy*. London, U.K.: Oxford, 1990.
[26] S. W. Grundfest, J. W. Burdick, and A. B. Slatkin, "The development of a robotic endoscope," in *Proc. IEEE Int. Conf. Robot. Autom.*, Nagoya, Japan, Aug. 1995, pp. 162–171.

ABD EL HAKEEM ABD EL NABY is currently an Associate Professor with the Department of Mathematics, Faculty of Science, Damietta University, Egypt. He has contributed significantly in the area of modeling and analysis of fluid mechanics and its applications. He has published several research articles in various leading journals.

A. H. EL-BAZ received the Ph.D. degree in computer science from Mansoura University, Egypt. He was a Postdoctoral Research Fellow with the Center for Soft Computing Research, Indian Statistical Institute, Kolkata, India, from March 2014 to August 2014; and a Visiting Researcher with the Faculty of Mathematics, Informatics and Mechanics, Warsaw University, Warsaw, Poland, in April 2016. He is currently an Associate Professor with the Department of Computer Science, Faculty of Computers and Artificial Intelligence, Damietta University, Egypt. He has published many papers in reputed journals and international conferences. His research interests include modeling, simulation, artificial intelligence, bioinformatics, and mathematical statistics and its applications. He is a member of many prestigious scientific societies. He got many distinguished scientific publication awards. He is also serving as a referee for many reputed international journals.